A high-order DG/FV convex property preserving scheme for hyperbolic systems with applications to shallow water flows and fluid-structure interaction

Sacha Cardonna[1], David Lannes[2], Fabien Marche[1] & François Vilar[1]

[1] *Institute of Mathematics Alexander Grothendieck, University of Montpellier, France*
[2] *Institute of Mathematics of Bordeaux, University of Bordeaux, France*

Applied Maths Colloquium of the University of Waterloo
Waterloo, Canada — March 2025

University of Waterloo | Department of Applied Mathematics

Université de Montpellier

IMAG — Institut Montpellierain Alexander Grothendieck

Overview of this talk

A **high-order DG/FV convex property preserving scheme** for **hyperbolic systems** with applications to **shallow water flows** and **fluid-structure interaction**

- **High-order DG/FV convex property preserving scheme**: combines an high-order scheme with a low-order invariant-domain-preserving scheme,
- **Hyperbolic systems**: systems of conservation laws modeling wave propagation phenomena,
- **Shallow water flows**: describe the water waves under the assumption that the vertical scale is negligible compared to the horizontal one,
- **Fluid-structure interaction**: coupling between fluid flow and a rigid floating object, with applications to coastal engineering, WEC, etc.

Table of contents

Slides available online at sachacardonna.github.io

Table of contents

Slides available online at sachacardonna.github.io

Hyperbolic systems in 2D

Generic system of conservation laws

Let $\Omega \subset \mathbb{R}^2$ be an open domain. We consider the following system of $m \geq 1$ conservation laws:

$$\boxed{\partial_t \boldsymbol{v}(\boldsymbol{x}, t) + \nabla_{\boldsymbol{x}} \cdot \mathbb{F}(\boldsymbol{v}, \boldsymbol{x}, t) = \boldsymbol{B}(\boldsymbol{v}, \boldsymbol{x}, t)}$$

- $\boldsymbol{v} : \Omega \times \mathbb{R}_+ \to \mathscr{A} \subset \mathbb{R}^m$ is the **conservative state vector**, where $\mathscr{A}$ is a convex set of admissible states,
- $\mathbb{F} : \mathscr{A} \times \Omega \times \mathbb{R}_+ \to (\mathbb{F}_x(\boldsymbol{v}, \boldsymbol{x}, t), \mathbb{F}_y(\boldsymbol{v}, \boldsymbol{x}, t))^\top \in \mathscr{M}_{2\times m}(\mathbb{R})$ is the **flux tensor**, with $\mathbb{F}_x, \mathbb{F}_y : \mathscr{A} \times \Omega \times \mathbb{R}_+ \to \mathbb{R}^m$,
- $\boldsymbol{B} : \mathscr{A} \times \Omega \times \mathbb{R}_+ \to \mathbb{R}^m$ is a generic geometric **source term**.

Such systems describe the evolution of **conserved quantities** (momentum, mass, energy, concentration, etc.) transported in space by fluxes. The divergence of the flux accounts for the exchange of these quantities through the boundary of any control volume, while the source term models production, loss, forcing or geometric effects.

Finite Volume & Discontinuous Galerkin frameworks

Finite Volume (FV)

- Integral formulation over control volumes $\omega_c \subset \Omega$ with $\Omega = \bigcup \omega_c$;
- Piecewise constant approximation:

$$\boldsymbol{v}_h^c(t) \simeq \frac{1}{|\omega_c|} \int_{\omega_c} \boldsymbol{v}(\boldsymbol{x}, t)\, d\boldsymbol{x},$$

  where $\boldsymbol{v}$ is the exact solution;
- Numerical flux $\mathbb{F}^*$ ensures conservation and stability.

✔ Robust and easy to implement, well-suited for nonlinear problems,

✖ Low-order accuracy unless polynomial reconstruction is applied.

Discontinuous Galerkin (DG)

- Weak formulation on each element $\omega_c \subset \Omega$ with $\Omega = \bigcup \omega_c$;
- Piecewise polynomial approx.:

$$\boldsymbol{v}_h^c(\boldsymbol{x}, t) = \sum_{m=1}^{\dim \mathbb{P}^k} \boldsymbol{v}_m^c(t)\, \psi_m^c(\boldsymbol{x}),$$

  with test functions in $\mathbb{P}^k(\omega_c)$;
- Numerical flux $\mathbb{F}^*$ to ensure local conservation.

✔ High-order accuracy with compact stencil, well-suited for parallelism,

✖ Less robust, more complex implementation and prone to oscillations.

Ideal setup for a generic hyperbolic system

For our purposes, an ideal numerical scheme for a generic system of conservation laws should be:

- **High-order accurate** to properly resolve smooth solutions and small-scale structures,
- **Shock-capturing** to robustly handle discontinuities and strong nonlinear effects,
- **Admissibility-preserving** to ensure that the numerical solution remains in the convex set $\mathscr{A}$ of physically admissible states,
- **Conservative** to guarantee the correct balance of fluxes across element interfaces,
- **Compatible with source terms** in order to correctly capture forcing, geometry, or relaxation effects,
- **Well-suited for unstructured meshes** to deal with complex geometries and realistic computational domains.

Table of contents

Slides available online at sachacardonna.github.io

Table of contents

Slides available online at sachacardonna.github.io

DG formulation through residuals

DG formulation for all $\psi_p^c \in \mathbb{P}^k(\omega_c)$

$$\sum_{m=1}^{N_k} \frac{d\boldsymbol{v}_m^c}{dt} \int_{\omega_c} \psi_m^c \psi_p^c \, d\boldsymbol{x} - \int_{\omega_c} \mathbb{F}(\boldsymbol{v}_h^c) \cdot \nabla_{\boldsymbol{x}} \psi_p^c \, d\boldsymbol{x} + \int_{\partial\omega_c} \mathbb{F}^* \cdot \boldsymbol{n} \, \psi_p^c \, dS = \int_{\omega_c} \boldsymbol{B} \psi_p^c \, d\boldsymbol{x}$$

Residual DG formulation for any basis function $\psi_m^c \in \mathbb{P}^k(\omega_c)$

$$\boxed{\mathbb{M}_c \frac{d\boldsymbol{V}_c}{dt} = \Phi_c + \boldsymbol{S}_c}$$

- $(\boldsymbol{V}_c)_m = \boldsymbol{v}_m^c(t)$ **solution moments**
- $(\mathbb{M}_c)_{mp} = \int_{\omega_c} \psi_m^c(\boldsymbol{x}) \, \psi_p^c(\boldsymbol{x}) \, d\boldsymbol{x}$ **local mass matrix**
- $(\Phi_c)_m = \int_{\partial\omega_c} \mathbb{F}^* \cdot \boldsymbol{n} \, \psi_p^c \, dS - \int_{\omega_c} \mathbb{F}(\boldsymbol{v}_h^c) \cdot \nabla_{\boldsymbol{x}} \psi_p^c \, d\boldsymbol{x}$ **DG residuals**
- $(\boldsymbol{S}_c)_m = \int_{\omega_c} \boldsymbol{B}(\boldsymbol{v}_h^c) \, \psi_p^c \, d\boldsymbol{x}$ **source term**

Stabilization principle

- **Classical stabilization:** apply limiters/a posteriori correction on the full cell

  ↪ risks **discarding** a mostly accurate solution due to a **local failure**

- **Subcell approach:** partition each cell into finer subcells to reduce the correction scale

  ↪ enabling a **surgical correction**, meaning only fix what's necessary, preserving as much of the high-order DG content as possible

Theory needed – Reformulation of DG as a subcell FV-like scheme

A little state-of-the-art on subcell stabilization and monolithic schemes

Generally, in subcell techniques, applying a **robust FV correction** on the **subgrid level** implies that **all the subcells** in the troubled cell are **impacted**.

Some pioneering references for this presentation

M. Sonntag & C. D. Munz, *Shock capturing for discontinuous Galerkin methods using finite volume subcells*. Finite Volumes for Complex Applications VII, pp. 945–953. Springer, 2014.

M. Dumbser & R. Loubère, *A simple robust and accurate a posteriori subcell finite volume limiter for the discontinuous Galerkin method on unstructured meshes*. J. Comp. Phys., 2016.

A. Rueda-Ramìrez, B. Bolm, D. Kuzmin & G. Gassner, *Monolithic convex limiting for Legendre-Gauss-Lobatto Discontinuous Galerkin Spectral-Element methods*. Commun. Appl. Math., 2024

Our approach: thanks to the **reconstructed flux** formalism, we can activate the correction **locally** on **non-admissible subcells only**!

↪ avoids wasting information in non-troubled regions and preserves accuracy.

Table of contents

Slides available online at sachacardonna.github.io

Mesh subdivision

Cell subdivision into $N_s \geq N_k$ subcells

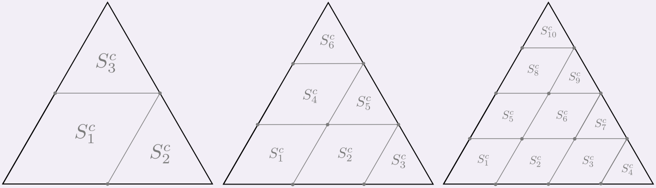

Cell ω_c subdivided into $N_s = N_k$ subcells for $\mathbb{P}^1$ (left), $\mathbb{P}^2$ (center) and $\mathbb{P}^3$ (right) cases

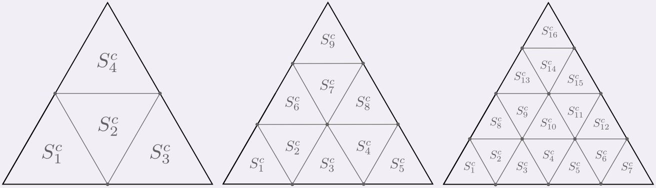

Cell ω_c subdivided into $N_s \geq N_k$ subcells for $\mathbb{P}^1$ (left), $\mathbb{P}^2$ (center) and $\mathbb{P}^3$ (right) cases

A classical mesh ...

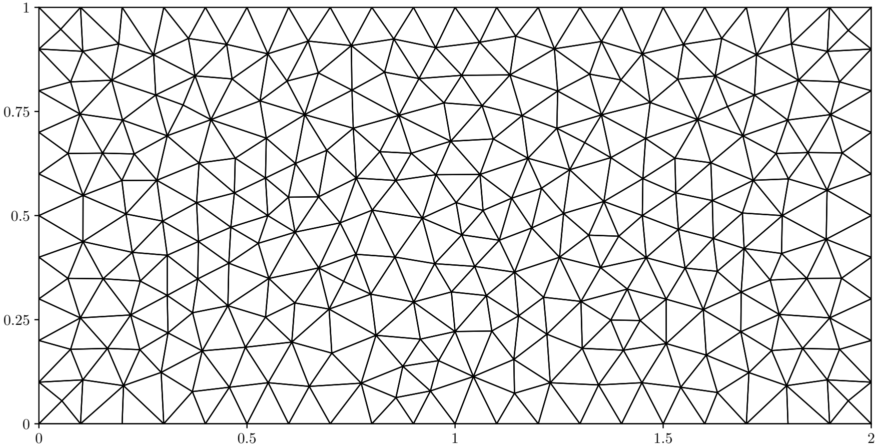

Figure: Unstructured simplicial mesh with $n_{\text{el}} = 350$ cells.

... and its subdivision

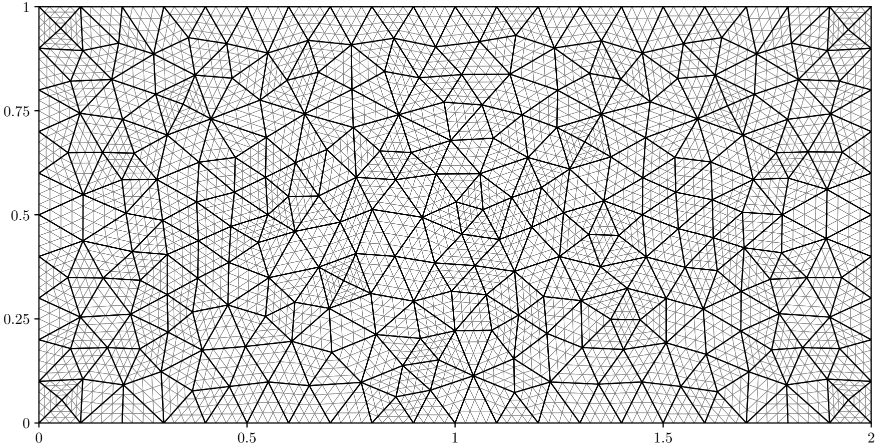

Figure: Unstructured simplicial mesh $\mathbb{P}^3$ subdivision onto triangles with $n_{\mathrm{el}} = 350$ cells.

Subdivision and submean values

Some notations

- For any element $\omega_c \in \mathcal{T}_h$, we define a sub-partition:

$$\mathcal{T}_{\omega_c} := \{S_1^c, \dots, S_{N_s}^c\}, \quad \overline{\omega}_c = \bigcup_{m=1}^{N_s} \overline{S}_m^c$$

- Γ_{mp}^c: interface between S_m^c and its neighbor S_p^v
- n_f^m: number of faces of subcell S_m^c
- $\mathcal{F}_{S_m^c}$: set of all faces of S_m^c
- n_f^c: total number of subcell faces inside element ω_c
- $\mathcal{V}_m^c$: set of face-neighboring subcells of S_m^c (with $|\mathcal{V}_m^c| = n_f^m$)
- $\breve{\mathcal{V}}_m^c$: subset of $\mathcal{V}_m^c$ containing only neighbors within the same element ω_c

Subneighbors

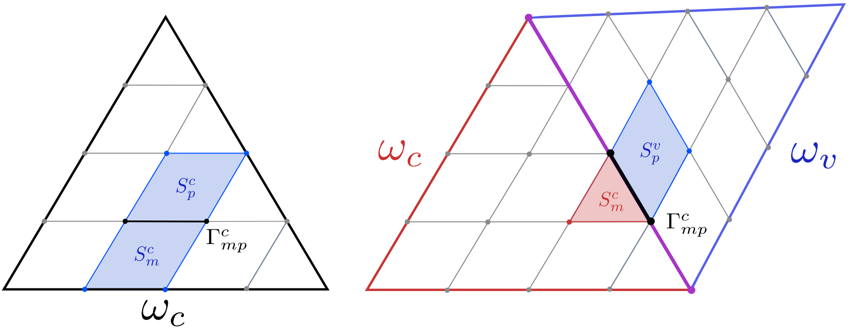

Figure: Two cases: subneighbor S_p inside cell ω_c (left), and subneighbor S_p inside neighbor cell ω_v (right).

Submean values and polynomial moments (1)

Mean value of a function over a subcell $S_m^c \subset \omega_c$

For any $f \in L^2(\omega_c)$, its submean value is $\overline{f}_m^c := \dfrac{1}{|S_m^c|} \displaystyle\int_{S_m^c} f(\boldsymbol{x})\, d\boldsymbol{x}$.

Submean values and projection matrix

- $(\overline{\boldsymbol{V}}_c)_m = \overline{\boldsymbol{v}}_m^c(t)$ **submean values**
- $(\mathbb{P}_c)_{mp} = \dfrac{1}{|S_m^c|} \displaystyle\int_{S_m^c} \psi_p^c(\boldsymbol{x})\, d\boldsymbol{x}$ **projection matrix**

$$\overline{\boldsymbol{v}}_m^c(t) = \frac{1}{|S_m^c|} \sum_{q=1}^{N_k} \boldsymbol{v}_q^c(t) \int_{S_m^c} \psi_q^c(\boldsymbol{x})\, d\boldsymbol{x} \implies \boxed{\overline{\boldsymbol{V}}_c = \mathbb{P}_c \boldsymbol{V}_c}$$

⚠ $\mathbb{P}_c^\top \mathbb{P}_c$ has to be **non-singular**, so we use the least-square procedure:

$$\boxed{\boldsymbol{V}_c = \left(\mathbb{P}_c^\top \mathbb{P}_c\right)^{-1} \mathbb{P}_c^\top \overline{\boldsymbol{V}}_c}$$

If $N_s = N_k$, then $\overline{\boldsymbol{V}}_c = \mathbb{P}_c \boldsymbol{V}_c \Leftrightarrow \boldsymbol{V}_c = \mathbb{P}_c^{-1} \boldsymbol{V}_c$.

Submean values and polynomial moments (2)

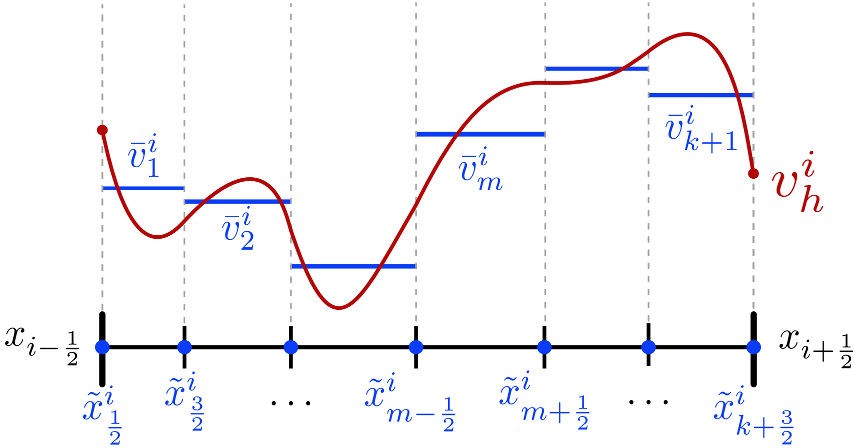

Figure: Piecewise polynomial function v_h^i and associated sub-mean-values (1D case).

Table of contents

Slides available online at sachacardonna.github.io

Reconstructed DG fluxes (1)

Submean values vector derivative

Since $\mathbb{M}_c \dfrac{d\boldsymbol{V}_c}{dt} = \Phi_c + \boldsymbol{S}_c$ and $\overline{\boldsymbol{V}}_c = \mathbb{P}_c \boldsymbol{V}_c \implies \boxed{\dfrac{d\overline{\boldsymbol{V}}_c}{dt} = \mathbb{P}_c \mathbb{M}_c^{-1}(\Phi_c + \boldsymbol{S}_c)}$

Flux reconstruction to get a FV-like scheme

Let us consider the DG reconstructed flux $\widehat{\mathbb{F}}_n$ such that

$$\frac{d\overline{\boldsymbol{v}}_m^c}{dt} = -\frac{1}{|S_m^c|}\int_{\partial S_m^c} \widehat{\mathbb{F}}_n(\boldsymbol{x})\,d\boldsymbol{x} + (\mathbb{P}_c\mathbb{M}_c^{-1}\boldsymbol{S}_c)_m \qquad \text{(FV-like scheme)}$$

$$= -\frac{1}{|S_m^c|}\sum_{S_p^v\in\mathcal{V}_m^c}\int_{\Gamma_{mp}^c} \widehat{\mathbb{F}}_n(\boldsymbol{x})\,d\boldsymbol{x} + (\mathbb{P}_c\mathbb{M}_c^{-1}\boldsymbol{S}_c)_m \qquad \left(\partial S_m^c = \cup_{S_p^v\in\mathcal{V}_m^c}\Gamma_{mp}^c\right)$$

$$= -\frac{1}{|S_m^c|}\left(\sum_{S_p^v\in\breve{\mathcal{V}}_m^c}\int_{\Gamma_{mp}^c} \widehat{\mathbb{F}}_n(\boldsymbol{x})\,d\boldsymbol{x} + \int_{\partial\omega_c\cap\partial S_m^c} \mathbb{F}_n^*\,d\boldsymbol{x}\right) + (\mathbb{P}_c\mathbb{M}_c^{-1}\boldsymbol{S}_c)_m$$

under the hypothesis that $\widehat{\mathbb{F}}_{n|\partial\omega} = \mathbb{F}^*$ for all $\omega \in \mathcal{T}_h$.

Reconstructed DG fluxes (2)

Interface reconstructed flux

We define $\widehat{\mathbb{F}}_{mp}$ at interface Γ^c_{mp} as: $\displaystyle\int_{\Gamma^c_{mp}} \widehat{\mathbb{F}}_n(\boldsymbol{x})\, d\boldsymbol{x} = \varepsilon^c_{mp}\widehat{\mathbb{F}}_{mp}$,

where subface orientation is carried through ε^c_{mp}, such that $\varepsilon^c_{pm} = -\varepsilon^c_{mp}$.

Reconstructed flux system

$$\boxed{-\mathbb{A}_c\widehat{\mathbb{F}}_c = \mathbb{D}_c\frac{d\overline{\boldsymbol{V}}_c}{dt} + \partial\mathbb{F}_c}$$

- $(\widehat{\mathbb{F}}_c)_{mp} = \ell_{mp}\widehat{\mathbb{F}}_{mp}$ **interior subfaces fluxes**
- $(\mathbb{A}_c)_{mp} = \varepsilon^c_{mp}$ **adjacency matrix**
- $(\mathbb{D}_c)_m = |S^c_m|$ **subvolume matrix**
- $(\partial\mathbb{F}_c)_m = \displaystyle\int_{\partial\omega_c\cap\partial S^c_m} \mathbb{F}^*_n\, d\boldsymbol{x}$ **cell boundary contribution**

⚠ Since $\ker\mathbb{A}_c \neq \{\mathbf{0}\}$, we use a *Graph Laplacian technique*

Reconstructed DG fluxes (3)

Residual definition of reconstructed fluxes

$$\boxed{\widehat{\mathbb{F}}_c = -\mathbb{A}_c^\top \mathscr{L}_c^{-1} \left(\mathbb{D}_c \mathbb{P}_c \mathbb{M}_c^{-1} \Phi_c + \partial \mathbb{F}_c\right)}$$

where $\mathscr{L}_c^{-1}$ is the gen. inverse of $\mathbb{L}_c := \mathbb{A}_c \mathbb{A}_c^\top$ on the orthogonal of its kernel:

$$\mathscr{L}_c^{-1} = (\mathbb{L}_c + \lambda \Pi)^{-1} - \frac{1}{\lambda}\Pi, \qquad \Pi = \frac{1}{N_s}(1 \otimes 1) \in \mathscr{M}_{N_k}, \qquad \forall \lambda \neq 0$$

R. Abgrall, *Some Remarks about Conservation for Residual Distribution Schemes*. Methods Appl. Math., 18:327-351, 2018.

Few remarks

- **Source term** is excluded in the definition since only flux-dependent integrals are considered in reconstruction,
- **Implementation**: only Φ_c and boundary terms $\partial \mathbb{F}_c$ depend on time, but all the other terms are precomputable,
- **Alternative expression**: using spanning set of subresolution functions $\phi_m^c = p_{\omega_c}^k(\mathbb{1}_m^c)$, where $p_{\omega_c}^k$ is the L^2-projector on cell ω_c.

DG schemes ≡ Subcell FV schemes

Theorem (equivalence of DG and subcell FV schemes)

The NSW-DG residual scheme $\frac{d\boldsymbol{V}_c}{dt} = \mathbb{M}_c^{-1}(\Phi_c + \boldsymbol{S}_c)$ can be recast into N_s FV-like subcell schemes as

$$\boxed{\frac{d\overline{\boldsymbol{V}}_c}{dt} = -\mathbb{D}_c^{-1}\left(\mathbb{A}_c\widehat{\mathbb{F}}_c + \partial\mathbb{F}_c\right) + \overline{\boldsymbol{S}}_c}$$

where $\overline{\boldsymbol{S}}_c := \mathbb{P}_c\mathbb{M}_c^{-1}\boldsymbol{S}_c$ contains the submean values of source term L^2-projection, i.e.

$$\overline{\boldsymbol{B}}_m^c := \frac{1}{|S_m^c|}\int_{S_m^c} p_{\omega_c}^k \circ \boldsymbol{B}(\boldsymbol{v}_h)\, d\boldsymbol{x}.$$

DG equiv. discrete scheme with FE time integration for all subcell $S_m^c \subset \omega_c$

$$\overline{\boldsymbol{v}}_m^{c,n+1} = \overline{\boldsymbol{v}}_m^{c,n} - \frac{\Delta t^n}{|S_m^c|}\sum_{S_p^v\in\mathcal{V}_m^c} \ell_{mp}\widehat{\mathbb{F}}_{mp} + \Delta t^n\overline{\boldsymbol{B}}_m^{c,n}, \qquad \forall m \in [\![1, N_s]\!]$$

Table of contents

Slides available online at sachacardonna.github.io

Combining DG and FV frameworks (1)

Finite Volume scheme 👍 robustness 👎 1^{st} order accuracy

$+$

Discontinuous Galerkin scheme 👍 k^{th}-order accuracy 👎 robustness

$\Downarrow$

Monolithic DG-FV subcell scheme 👍 k^{th}-order accuracy & robustness

Combining DG and FV frameworks (2)

Our numerical solution should satisfy the following properties:

- **Accuracy**: high-order precision can be required
  $\hookrightarrow$ natural in DG schemes; requires mesh refinement in FV schemes
- **Physical admissibility**: the solution should stay in the admissibility set $\mathscr{A}$
  $\hookrightarrow$ automatic in FV schemes; requires dedicated techniques in DG schemes
- **Stability / No spurious oscillations**: satisfy a discrete maximum principle
  $\hookrightarrow$ guaranteed in FV schemes; not ensured by DG schemes (limiters needed)

Idea – blending DG reconstructed fluxes and FV fluxes at subcell scale

Combining DG and FV frameworks (3)

Blended fluxes and blending coefficient

For every face $\Gamma^c_{mp} \in \mathscr{F}_{S^c_m}$, the high-order DG reconstructed flux $\widehat{\mathbb{F}}_{mp}$ and a first-order FV flux $\mathbb{F}^{*,\mathrm{FV}}_{mp}$ are assembled in a convex way:

$$\boxed{\widetilde{\mathbb{F}}_{mp} = \mathbb{F}^{*,\mathrm{FV}}_{mp} + \Theta_{mp}\left(\widehat{\mathbb{F}}_{mp} - \mathbb{F}^{*,\mathrm{FV}}_{mp}\right) = \mathbb{F}^{*,\mathrm{FV}}_{mp} + \Theta_{mp}\Delta\mathbb{F}_{mp}}$$

⚠ The **blending coefficient** $\Theta_{mp} \in [0,1]$ is:

- computed *a priori* on each Γ^c_{mp}, at each time step (or RK stage),
- uniquely defined *i.e.* $\Theta_{mp} = \Theta_{pm}$, for all $S^v_p \in \mathscr{V}^c_m$.

Monolithic DG-FV subcell scheme with FE time integration

$$\overline{\boldsymbol{v}}^{c,n+1}_m = \overline{\boldsymbol{v}}^{c,n}_m - \frac{\Delta t^n}{|S^c_m|} \sum_{S^v_p \in \mathscr{V}^c_m} \ell_{mp}\widetilde{\mathbb{F}}_{mp} + \Delta t^n \overline{\boldsymbol{B}}^{c,n}_m, \qquad \forall m \in [\![1, N_s]\!]$$

Table of contents

Slides available online at sachacardonna.github.io

A first shallow water asymptotic model

Nonlinear shallow water (NSW) equations

$$\boxed{\partial_t \boldsymbol{v} + \nabla_{\boldsymbol{x}} \cdot \mathbb{F}(\boldsymbol{v}, b) = \boldsymbol{B}[b](\boldsymbol{v})}$$

- $b : \mathbb{R}^2 \to \mathbb{R}$ is the **topography** parametrization,
- $\boldsymbol{v} : \mathbb{R}^2 \times \mathbb{R}_+ \to \mathscr{H}_b^+$ is the vector gathering **total elevation** η and **discharge** $\boldsymbol{q} := (q_x, q_y)^\top$, with $\mathscr{H}_b^+ = \{(\eta, q_x, q_y) \in \mathbb{R}^3 \mid \eta - b \geq 0\}$,
- $\mathbb{F} : \mathscr{H}_b^+ \times \mathbb{R} \to (\boldsymbol{q},\ \boldsymbol{u} \otimes \boldsymbol{q} + \frac{g\eta}{2}(\eta - 2b)\mathbb{I}_2)^\top \in \mathscr{M}_{2\times 3}(\mathbb{R})$ is the nonlinear **flux** tensor,
- $\boldsymbol{B} : \mathscr{H}_b^+ \to (0, -g\eta\nabla_{\boldsymbol{x}} b)^\top \in \mathbb{R}^3$ is the **topography source term**.

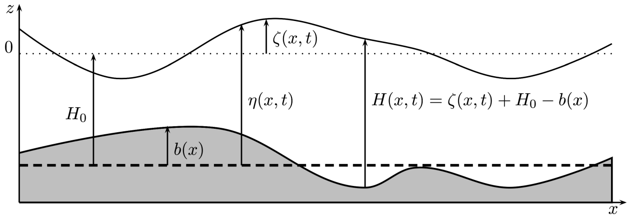

Table of contents

Slides available online at sachacardonna.github.io

Source term treatment

Flowchart of the discretization

Dealing with both **polynomial DOFs** and **subcell-averaged values**

1. **Subcell averages**: compute the submean values of the quantities involved on each subcell, then reconstruct polynomials via projection matrix $\mathbb{P}_c$,
2. **Projection**: evaluate $\boldsymbol{B}(\boldsymbol{v}_h)$ at quadrature nodes, then apply an L^2 projection onto $\mathbb{P}^k$,
3. **Integration**: compute the mean value of the projected source over each subcell:

$$\overline{\boldsymbol{B}}_m^c := \frac{1}{|S_m^c|} \int_{S_m^c} \boldsymbol{B}_h \, d\boldsymbol{x}$$

Implementation remark

Formally corresponds to multiplying the DG source integral by $\mathbb{P}_c \mathbb{M}_c^{-1}$:

$$\overline{\boldsymbol{B}}_m^c = \mathbb{P}_c \mathbb{M}_c^{-1} \left(\int_{\omega_c} \boldsymbol{B}_h \varphi_h \, d\boldsymbol{x} \right)$$

Generalization to algebraic/geometric source terms

Topography and (nonlinear) friction effects

$$\boxed{\boldsymbol{S}[b](\boldsymbol{v}) := \boldsymbol{B}[b](\boldsymbol{v}) + \boldsymbol{R}[b](\boldsymbol{v})}$$

- $\boldsymbol{B}[b](\boldsymbol{v}) = (0, -g\eta\nabla_{\boldsymbol{x}} b)^\top$ **Topography source term**
- $\boldsymbol{R}[b](\boldsymbol{v}) = \begin{cases} \left(0, -k_f^2\, \boldsymbol{q}\right)^\top, \ k_f > 0 \\ \left(0, -n_f^2 \dfrac{\boldsymbol{q}\,\|\boldsymbol{q}\|}{(\eta - b)^\gamma}\right)^\top, \ n_f, \gamma > 0 \end{cases}$ **Linear friction law** / **Manning friction law**

Handled the same way as previously → **easily generalizable**

Applications to Serre–Green–Naghdi (SGN) dispersive equations

Reformulation: Elliptic problem + NSW with dispersive source term

1. Elliptic problem solved *independently*, using a finite element method;
2. Resulting dispersive source term discretized within the NSW framework.

Table of contents

Slides available online at sachacardonna.github.io

Reformulation as a Godunov-like scheme

Solution at t^{n+1} as a convex combination of quantities defined at t^n

$$\overline{\boldsymbol{v}}_m^{c,n+1} = \overline{\boldsymbol{v}}_m^{c,n} - \frac{\Delta t^n}{|S_m^c|} \sum_{S_p^v \in \mathcal{V}_m^c} \ell_{mp} \widetilde{\mathbb{F}}_{mp} + \Delta t^n \overline{\boldsymbol{B}}_m^{c,n}$$

$$+ \frac{\Delta t^n}{|S_m^c|} \mathbb{F}\left(\overline{\boldsymbol{v}}_m^{c,n}\right) \cdot \sum_{S_p^v \in \mathcal{V}_m^c} \ell_{mp} \boldsymbol{n}_{mp} \pm \frac{\sigma \Delta t^n}{|S_m^c|} \sum_{S_p^v \in \mathcal{V}_m^c} \ell_{mp} \overline{\boldsymbol{v}}_m^{c,n}$$

$$= \left(1 - \frac{\sigma \Delta t^n}{|S_m^c|} \sum_{S_p^v \in \mathcal{V}_m^c} \ell_{mp}\right) \overline{\boldsymbol{v}}_m^{c,n} + \frac{\sigma \Delta t^n}{|S_m^c|} \sum_{S_p^v \in \mathcal{V}_m^c} \ell_{mp} \widetilde{\boldsymbol{v}}_{mp}^{*,-} + \Delta t^n \overline{\boldsymbol{B}}_m^{c,n}$$

- $\widetilde{\boldsymbol{v}}_{mp}^*$ are the **blended Riemann intermediate states**

$$\widetilde{\boldsymbol{v}}_{mp}^* := \overline{\boldsymbol{v}}_m^{c,n} - \frac{\widetilde{\mathbb{F}}_{mp} - \mathbb{F}\left(\overline{\boldsymbol{v}}_m^{c,n}\right) \cdot \boldsymbol{n}_{mp}}{\sigma} = \boldsymbol{v}_{mp}^* - \Theta_{mp} \left(\frac{\widehat{\mathbb{F}}_{mp} - \mathbb{F}_{mp}^{*,\mathrm{FV}}}{\sigma}\right);$$

- $\boldsymbol{v}_{mp}^*$ are the 1^{st}-**order FV Riemann intermediate states**.

Analytical formula to ensure water height positivity

Relying on 1^{st}-order FV Riemann intermediate states

Proof of the natural **preservation of water-height positivity** for 1^{st}-order elevation Riemann FV states $\eta_{mp}^{*,\pm}$

↪ allows us to rely on the **robustness of FV framework** to ensure the properties we want

Physical admissibility detector

$$\boxed{\Theta_{mp}^{\mathscr{H}_b^+} := \min\left(\Theta_{mp}^{\mathscr{H}_b^+,-}, \Theta_{mp}^{\mathscr{H}_b^+,+}\right)}$$

- $\Theta_{mp}^{\mathscr{H}_b^+,-} := \dfrac{\sigma\left(\eta_{mp}^* - \overline{b}_m^c\right)}{\Delta\mathbb{F}_{mp}}$ if $\Delta\mathbb{F}_{mp} > 0$, $\quad \Theta_{mp}^{\mathscr{H}_b^+,-} = 1$ else;
- $\Theta_{mp}^{\mathscr{H}_b^+,+} := \dfrac{\sigma\left(\overline{b}_p^v - \eta_{mp}^*\right)}{\Delta\mathbb{F}_{pm}}$ if $\Delta\mathbb{F}_{pm} < 0$, $\quad \Theta_{mp}^{\mathscr{H}_b^+,+} = 1$ else.

Analytical formula to prevent spurious oscillations

Mimicking a local maximum principle

$$\alpha_m^c := \min_{S_p^v \in \mathcal{N}(S_m^c)} \overline{\eta}_p^{v,n} \leq \overline{\eta}_m^{c,n+1} \leq \max_{S_p^v \in \mathcal{N}(S_m^c)} \overline{\eta}_p^{v,n} =: \beta_m^c$$

where $\mathscr{P}_m^c$ is the set of vertices $\boldsymbol{x}_p$ of subcell S_m^c and

$$\mathcal{N}(S_m^c) := \bigcup_{\boldsymbol{x}_p \in \mathscr{P}_m^c} \{S_q \mid \boldsymbol{x}_p \in S_q\}$$

Subcell numerical admissibility detector

$$\Theta_{mp}^{\text{SubNAD}} := \min\left(1, \left|\frac{\sigma}{\Delta\mathbb{F}_{mp}}\right| \begin{cases} \min\left(\beta_p^v - \eta_{mp}^{*,+},\ \eta_{mp}^{*,-} - \alpha_m^c\right) & \text{if } \Delta\mathbb{F}_{mp} > 0 \\ \min\left(\beta_m^c - \eta_{mp}^{*,-},\ \eta_{mp}^{*,+} - \alpha_p^v\right) & \text{if } \Delta\mathbb{F}_{mp} < 0 \end{cases}\right)$$

⚠ For NSW, no local maximum principle for the conserved variable!

↪ needs to be **relaxed** in the presence of **smooth extremas**

Table of contents

Slides available online at sachacardonna.github.io

Preservation of steady-states (1)

Why does it matter ?

- **Preserves lake at rest steady states exactly**, avoiding spurious motions;
- **Reduces numerical errors** near equilibrium, especially when small perturbations are present;
- **Essential for wet/dry interfaces**, where small oscillations can destabilize the scheme.

Well-balancing (WB) property

Providing that the integrals of discrete formulation are exactly computed, we have the following result:

$$\forall n \in \mathbb{N}, \quad \forall \eta^e > 0, \quad (\eta_h^n = \eta^e \text{ and } \boldsymbol{q}_h^n = \mathbf{0}) \Longrightarrow \left(\eta_h^{n+1} = \eta^e \text{ and } \boldsymbol{q}_h^{n+1} = \mathbf{0}\right)$$

Preservation of steady-states (2)

Sketch of proof

Objective: showing that numerical fluxes are cancelling the source term *i.e.*

$$\frac{1}{|S_m^c|} \sum_{S_p^v \in \mathcal{V}_m^c} \ell_{mp} \widetilde{\mathbb{F}}_{mp} = \overline{\boldsymbol{B}}_m^{c,n} \qquad \text{s.t.} \qquad \overline{\boldsymbol{v}}_m^{c,n+1} = \overline{\boldsymbol{v}}_m^{c,n}.$$

- Exact integration required → natural with high-order quadrature;
- Under well-balanced assumptions:

$$\nabla_{\boldsymbol{x}} \cdot \mathbb{F}(\boldsymbol{v}_c, b_c) = \boldsymbol{B}(\boldsymbol{v}_c, \nabla_{\boldsymbol{x}} b_c), \quad \forall \omega_c \in \mathcal{T}_h;$$

- Fluxes $\widehat{\mathbb{F}}_{mp}$ and $\mathbb{F}_{mp}^{*,\text{FV}}$ match the continuous flux $\mathbb{F}_h^c \cdot \boldsymbol{n}_{mp}$ under equilibrium;
- $\widetilde{\mathbb{F}}_{mp}$ is built as a convex combination of these well-balanced fluxes ↪ preserves equilibrium as well !

Table of contents

Slides available online at sachacardonna.github.io

Test 1 – Order of accuracy assessment

Steady vortex with $\mathscr{C}^\infty$ topography

- **Domain:** $\Omega = [-5,5]^2$ **Degree:** $k = 1,2,3$ **Mesh:** $n_{\text{el}} = 200 \to 12800$
- **Goal:** convergence of the scheme on a smooth solution with a consistent discretization of the topography source term

k	1		2		3	
h	$E^\eta_{L^2}$	$q^\eta_{L^2}$	$E^\eta_{L^2}$	$q^\eta_{L^2}$	$E^\eta_{L^2}$	$q^\eta_{L^2}$
1	9.445E-2	2.35	1.529E-2	2.91	4.580E-3	4.19
$\frac{1}{2}$	1.854E-2	2.16	2.039E-3	3.03	2.505E-4	4.10
$\frac{1}{4}$	4.158E-3	2.07	2.491E-4	2.97	1.465E-5	4.00
$\frac{1}{8}$	9.923E-4	–	3.187E-5	–	9.165E-7	–

Figure: L^2-errors between numerical and analytical solutions and convergence rates for η at time $t = 0.1$ sec.

Test 2 – Riemann problem

Dam-break on a wet bed

- **Domain:** $\Omega = [0, 1000] \times [0, 200]$ **Degree:** $k = 4$ **Mesh:** $n_{\text{el}} = 350$
- **Goal:** handling shock waves and rarefaction fronts

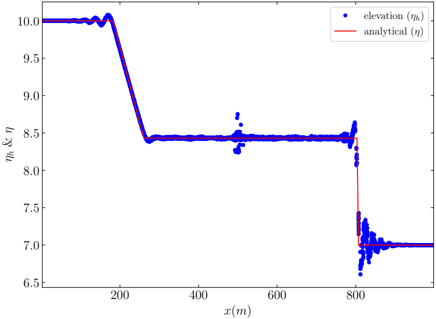

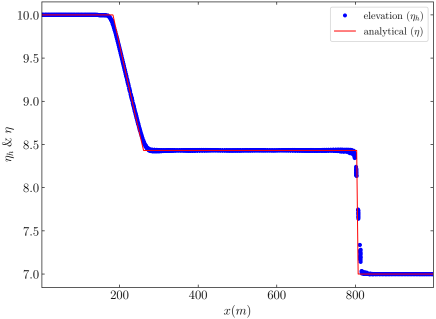

Figure: At $t = 32$ sec, $\mathbb{P}^4$ pure DG elevation (left) and monolithic DG/FV subcells elevation (right).

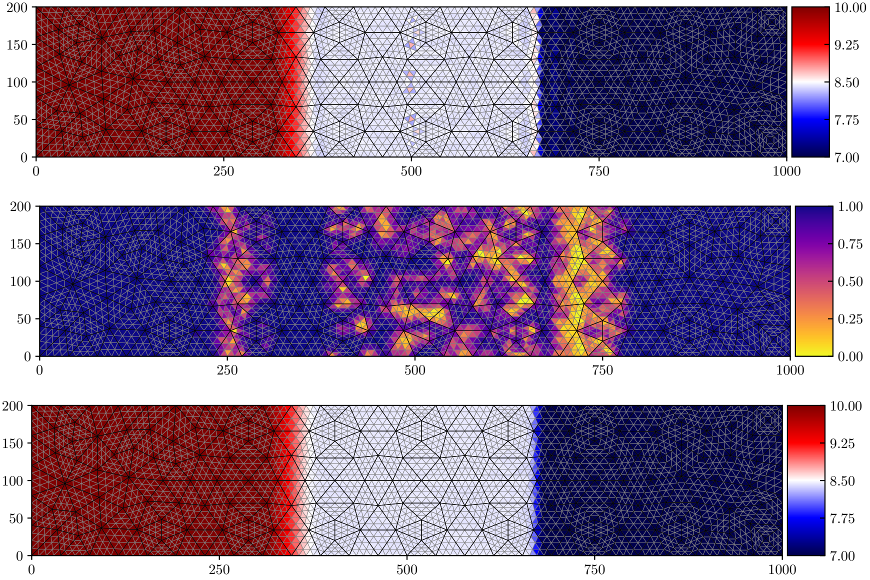

Figure: At $t = 18$ sec, $\mathbb{P}^4$ unlimited DG elevation (top), map of blending coefficient means per subcell (center) and monolithic DG/FV subcells elevation (bottom).

Test 3 – Periodic run-up/run-down

Carrier & Greenspan periodic solution

- **Domain:** $\Omega = [-20, 6] \times [0, 4]$ **Degree:** $k = 2$ **Mesh:** $n_{\text{el}} = 1092$
- **Goal:** assessing the ability of the scheme to capture periodic solutions on a dry bed with no phase shift

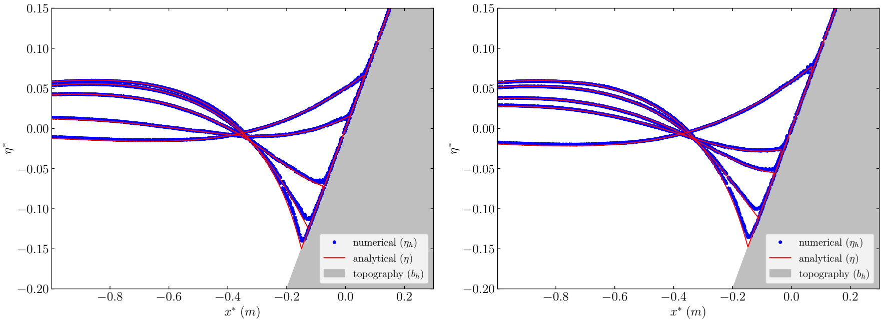

Figure: Snapshots of $\mathbb{P}^2$ elevation for $t \in [80, 86]$ sec (left) and for $t \in [154, 160]$ sec (right).

Test 4 — Rock-wave interactions

Single wave collapsing on a Gaussian rock

- **Domain:** $\Omega = [5, 25] \times [0, 30]$ **Degree:** $k = 6$ **Mesh:** $n_{\text{el}} = 584$
- **Goal:** assessing robustness and correct shock-capturing in challenging case

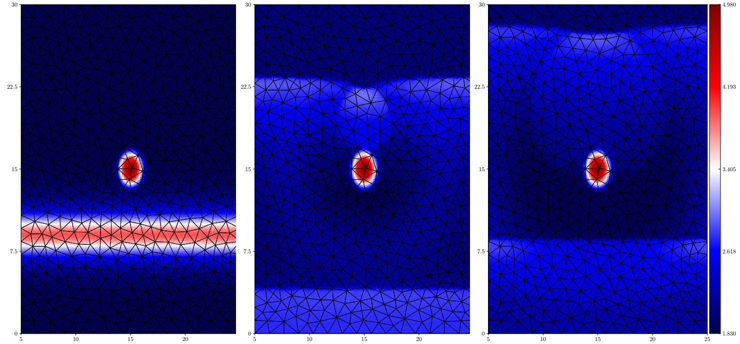

Figure: Snapshots of $\mathbb{P}^6$ elevation at several times (and link to simulation).

Table of contents

Slides available online at sachacardonna.github.io

Few words about wave–structure interactions

Why are we interested in wave–structure interactions?

- Offshore engineering (WEC, floating platforms, coastal protection),
- Understanding nonlinear wave dynamics under geometric constraints,
- Designing predictive and efficient simulation tools.

Mathematical and numerical challenges

- Strong nonlinear coupling between fluid and structure,
- Moving interfaces and transmission conditions,
- Delicate well-posedness issues depending on the chosen formulation.

Two modeling approaches

- **Engineering-oriented models**: more flexible, sometimes less rigorous, but able to capture complex configurations and go further in practice,
- **Mathematically-structured models**: derived with stronger analytical control, ensuring consistency and stability, at the price of additional constraints and technical complexity ← *we're here* ☺

Table of contents

Slides available online at sachacardonna.github.io

3D setting

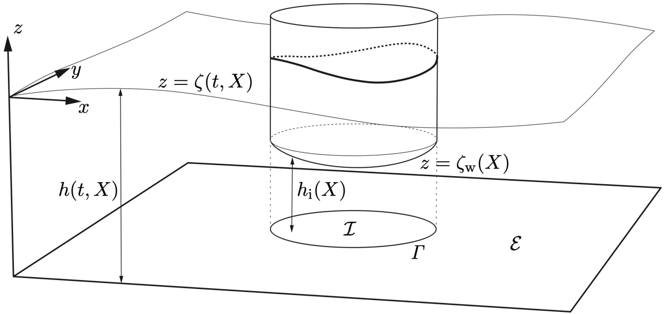

- Fluid domain bounded below by a flat bottom and above by a free surface $z = \zeta(\boldsymbol{x}, t)$,
- A rigid, stationnary, partially immersed floating structure interacts with the surrounding flow,
- Vertical variations are averaged, leading to shallow-water type models.

2D horizontal setting

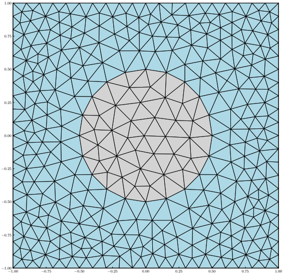
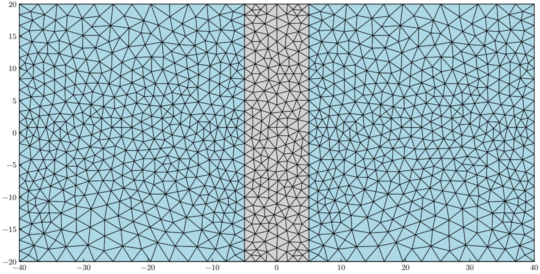

Figure: Two type of configurations: cylinder object and pontoon-like object.

For the latter numerical resolution, we will work in a 2D horizontal setting, where the domain is decomposed into three parts:

- Ω_s ("solid region"): hor. projection of the wet part under the object,
- Ω_f ("fluid region"): hor. projection of the free surface in contact with air,
- Ω_{fs}: interface separating them, with unit normal $\boldsymbol{n}$ pointing toward Ω_f.

Table of contents

Slides available online at sachacardonna.github.io

A new wave–structure interaction model

Exterior hyperbolic problem with boundary coupling

- Exterior region Ω_f (free surface):

$$\begin{aligned} \partial_t \zeta + \nabla_{\boldsymbol{x}} \cdot (H\boldsymbol{u}) &= 0 \\ \partial_t \boldsymbol{u} + \nabla_{\boldsymbol{x}}\big(\mathrm{g}\zeta + \tfrac{1}{2}|\boldsymbol{u}|^2\big) &= \boldsymbol{0} \end{aligned}$$

Nonlinear shallow-water equations

- Interior region Ω_s (object):

$$\begin{aligned} \nabla_{\boldsymbol{x}} \cdot \big(H^s \nabla_{\boldsymbol{x}} \phi^s\big) &= 0 \quad \text{in } \Omega_s \\ \phi^s &= \psi^s \quad \text{on } \Omega_{fs} \end{aligned}$$

Elliptic equation on potential

- Interface Ω_{fs} (boundary coupling):

$$\boldsymbol{n} \cdot (H\boldsymbol{u}) = \Lambda\psi^s, \quad \Lambda\psi^s := H^s \nabla_{\boldsymbol{x}} \phi^s \cdot \boldsymbol{n}$$

Dirichlet–Neumann operator

$$\partial_t \psi^s = -\mathrm{g}\zeta - \tfrac{1}{2}|\boldsymbol{u}|^2$$

Bernoulli ODE

- Initial conditions: $(\zeta, \boldsymbol{u})_{|t=0} = (\zeta^{\mathrm{in}}, \boldsymbol{u}^{\mathrm{in}})$ in Ω_f and $\psi^s_{|t=0} = \psi^s_{\mathrm{in}}$ on Ω_{fs}.

A new wave–structure interaction numerical coupling

How equations talk to each other

1. The following ODE is solved reading the values of ζ and $\boldsymbol{u}$ at the interface

$$\partial_t \psi^s = -g\zeta - \frac{1}{2}|\boldsymbol{u}|^2 \quad \text{on } \Omega_{fs} \qquad \textbf{SSP-RK scheme}$$

2. The trace ψ^s is used as a Dirichlet boundary condition to solve the interior elliptic problem

$$\begin{aligned} \nabla_{\boldsymbol{x}} \cdot \left(H^s \nabla_{\boldsymbol{x}} \phi^s\right) &= 0 \quad \text{in } \Omega_s \\ \phi^s &= \psi^s \quad \text{on } \Omega_{fs} \end{aligned} \qquad \textbf{Hybrid High-Order scheme}$$

3. The normal flux at the interface is computed from the Dirichlet–Neumann operator $\Lambda\psi^s := H^s \nabla_{\boldsymbol{x}} \phi^s \cdot \boldsymbol{n}$ and used as a boundary condition for the exterior hyperbolic problem in Ω_f:

$$\begin{aligned} \partial_t \zeta + \nabla_{\boldsymbol{x}} \cdot (H\boldsymbol{u}) &= 0 \\ \partial_t \boldsymbol{u} + \nabla_{\boldsymbol{x}}\left(g\zeta + \frac{1}{2}|\boldsymbol{u}|^2\right) &= \boldsymbol{0} \end{aligned} \qquad \textbf{Monolithic DG/FV scheme}$$

↪ The time integration is handled using a **SSP-RK scheme**.

Table of contents

Slides available online at sachacardonna.github.io

Finally, some waves

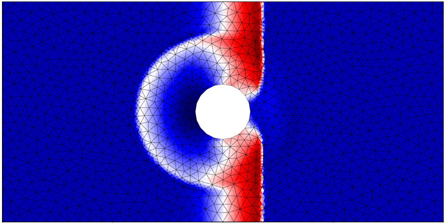

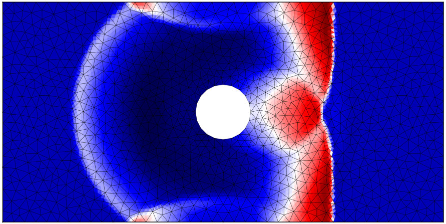

1. Wave propagation under a fixed floating structure (MP4),
2. Wave hitting a fixed submerged cylinder obstacle (MP4),
3. Wave hitting a submerged moving pontoon object (MP4),
4. Wave generation by a prescribed motion of the floating structure (MP4).

↪ More simulations on my webpage!

Table of contents

Slides available online at sachacardonna.github.io

Ongoing and upcoming work

What has been done...

S.C., A. Haidar, F. Marche & F. Vilar, *Local subcell monolithic DG/FV methods for nonlinear SW models with source terms*. IJNMF (rev.), 2026.

S.C., F. Marche & F. Vilar, *An high-order scheme for 2D NSW equations with topography and friction effects on unstructured grids*. JCP (rev.), 2026.

S.C., D. Lannes, F. Marche & F. Vilar, *Numerical resolution of 2D NSW equations with a partly immersed surface obstacle*. In preparation. 2026.

... and what are the plans for the future!

- Designing a model taking into account the **free motion** of the structure,
- Adaptation of the method to **moving** or **deforming** meshes via an **ALE framework**,
- Extension to **dispersive water-waves equations** (e.g. Green–Naghdi, Boussinesq) to capture more complex wave phenomena.

∼ Thank you for your attention! ∼

Special acknowledgments

- **Applied Mathematics Group of UW**
  ↪ especially *D. Del Rey Fernández* for the invitation! ☺
- **My mentors and advisors**
  ↪ *F. Marche & F. Vilar*
- **Supportive professors**
  ↪ *A. Duran, D. Lannes, B. Mohammadi, P. Azerad & D. Le Roux*
- **Colleagues and friends**
  ↪ *A. Haidar & M. Hanot*

Contact: *sacha.cardonna@umontpellier.fr*
Website: *sachacardonna.github.io*

Quadrature on subcells

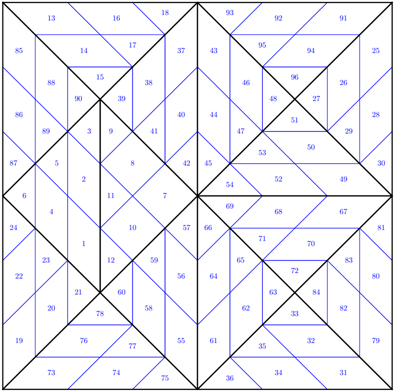

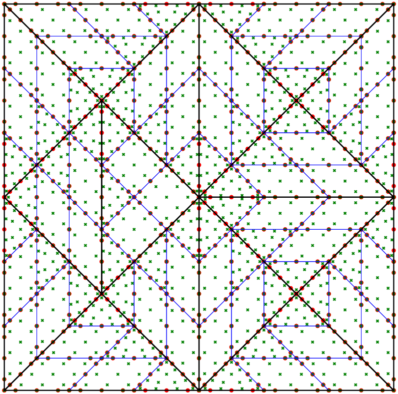

Figure: Subdivision of a coarse mesh into subcells with their global numbering (left), alongside the quadrature points for subcell interiors and faces (right).

Initialization

Initialization strategy

Initialization is performed via **subcell averages** followed by projection using $\mathbb{P}_c$, instead of L^2 projection or interpolation as usually done in DG schemes

$\hookrightarrow$ this guarantees $\boldsymbol{v}_h \in \mathscr{H}_b^+$ at $t = 0$, and enforces $\eta_h = b_h$ in dry zones

⚠ Since b_h is discontinuous across cells, **hydrostatic reconstruction** is applied to both DG and subcell FV fluxes.

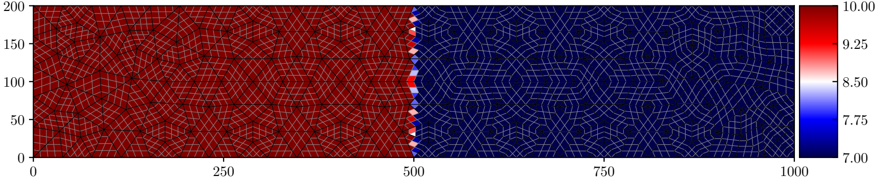

Figure: $\mathbb{P}^3$ dam-break problem initialization.

Hydrostatic reconstruction

Assuring both WB and positivity in numerical fluxes

❓ Hydrostatic reconstruction framework used on both DG and subcell FV fluxes
↪ ensures **positivity** of the water height, even for discontinuous topography

At each interface $\Gamma_{cv(k)}$ (resp. subinterface $\Gamma_{mp(k)}$), reconstructed values are defined:

- Topography rec.: $\widetilde{b}_k = \max(b_k^-, b_k^+)$, $\check{b}_k = \widetilde{b}_k - \max(0, \widetilde{b}_k - \eta_k^-)$
- Water height/elevation rec.: $\check{H}_k^\pm = \max(0, \eta_k^\pm - \widetilde{b}_k)$, $\check{\eta}_k^\pm = \check{H}_k^\pm + \widetilde{b}_k$
- Modified states: $\check{\boldsymbol{v}}_k^\pm = \left(\check{\eta}_k^\pm, \dfrac{\check{H}_k^\pm}{H_k^\pm}\boldsymbol{q}_k^\pm\right)^\top$

These are then used in a Lax-Friedrichs-type flux $\mathbb{F}^*$, completed by a correction term $\check{\mathbb{F}}_{cv(k)}$ to ensure well-balancing:

$$\mathbb{F}^*_{cv(k)} = \mathbb{F}^*(\check{\boldsymbol{v}}_k^-, \check{\boldsymbol{v}}_k^+, \check{b}_k, \check{b}_k, \boldsymbol{n}_{cv(k)}) + \check{\mathbb{F}}_{cv(k)}$$

Source term treatment

Alternative discretization of the topography source term

$$\boxed{\overline{\boldsymbol{B}}_m^c = \overline{\boldsymbol{B}}_m^{c,\mathrm{FV}} + \Theta_m^c \left(\overline{\boldsymbol{B}}_m^{c,\mathrm{DG}} - \overline{\boldsymbol{B}}_m^{c,\mathrm{FV}} \right)}$$

- $\Theta_m^c = \dfrac{1}{\#\mathcal{V}_m^c} \displaystyle\sum_{S_p^v \in \mathcal{V}_m^c} \Theta_{mp}$ **subcell global blending**
- $\overline{\boldsymbol{B}}_m^{c,\mathrm{DG}} = \dfrac{1}{|S_m^c|} \displaystyle\int_{S_m^c} \boldsymbol{B}_h^c \, d\boldsymbol{x}$ **DG source term**
- $\overline{\boldsymbol{B}}_m^{c,\mathrm{FV}} = \dfrac{1}{|S_m^c|} \displaystyle\int_{S_m^c} \boldsymbol{B}[b_h^c](\overline{\boldsymbol{v}}_m^c) \, d\boldsymbol{x}$ **FV source term**

No significant difference in results $\rightarrow$ we keep $\overline{\boldsymbol{B}}_m^c = \overline{\boldsymbol{B}}_m^{c,\mathrm{DG}}$

Blending relaxation

Smoothness detector on subcells

⚠ Must ensure to **relax correction** close to **smooth extremas**!

1. **Linearized reconstructions** of $\partial_x \eta_h$ and $\partial_y \eta_h$ are built inside subcell, i.e.

$$\mathfrak{E}_x^m(\boldsymbol{x}) := \overline{\partial_x \eta_h^c}^m + \overline{\nabla_{\boldsymbol{x}}(\partial_x \eta_h^c)}^m \cdot (\boldsymbol{x} - \boldsymbol{x}_m^c),$$
$$\mathfrak{E}_y^m(\boldsymbol{x}) := \overline{\partial_y \eta_h^c}^m + \overline{\nabla_{\boldsymbol{x}}(\partial_y \eta_h^c)}^m \cdot (\boldsymbol{x} - \boldsymbol{x}_m^c),$$

2. **Checking these indicators values at vertices**: if their values remain within the local extrema over a stencil, the solution is considered smooth over subcell S_m^c;
3. **If two neighbors S_m^c and S_p^v are considered smooth**, the blending coefficient on Γ_{mp} is relaxed to $\Theta_{mp} = 1 \rightarrow$ **full DG accuracy**

When to use the smooth extrema detector?

- **Order $\leq$ 2:** No detector needed.
- **Order $=$ 3:** Detector required at the **cell** level.
- **Order $\geq$ 4:** Detector required at the **subcell** level.

Blending smoothening

Why smoothening blending coefficient?

A **sharp switch** between low and high-order fluxes (i.e., $\Theta_{mp} = 0$ vs. $\Theta_{mp} = 1$) may cause **local oscillations**
$\hookrightarrow$ blending smoothers designed to **mitigate abrupt transitions**

- **Mean-value smoother** (default in experiments):

$$\Theta_m^c := \frac{1}{\#\mathcal{V}_m^c} \sum_{S_p^v \in \mathcal{V}_m^c} \Theta_{mp}, \quad \widetilde{\Theta}_{mp} := \min\left(\Theta_{mp}, \frac{1}{\#\mathcal{V}_{mp}} \sum_{S_q^v \in \mathcal{V}_{mp}} \Theta_q^v\right)$$

$\hookrightarrow$ Less diffusive, smoother transitions

- **Minimum-value smoother**:

$$\Theta_m^c := \min_{S_p^v \in \mathcal{V}_m^c} \Theta_{mp}, \quad \widetilde{\Theta}_{mp} := \min\left(\Theta_{mp}, \min_{S_q^v \in \mathcal{V}_{mp}} \Theta_q^v\right)$$

$\hookrightarrow$ Stronger damping near discontinuities

Constraints induced by the floating object

Exterior region Ω_f (free surface)

- Flow governed by NSW eq.,
- Pressure is prescribed: $\underline{\mathrm{p}} = \mathrm{p}_{\mathrm{atm}}$,
- The NSW momentum equation has no source term:

$$\partial_t \boldsymbol{u} + \boldsymbol{u} \cdot \nabla_{\boldsymbol{x}} \boldsymbol{u} + \mathrm{g} \nabla_{\boldsymbol{x}} \zeta = \mathbf{0}.$$

Interior region Ω_s (under the object)

- Free surface is blocked by the object (underwater part of the structure),
- Elevation is prescribed: $\zeta^s = \zeta^{\mathrm{w}}$,
- Leads to an "incompressible" constraint: $\nabla_{\boldsymbol{x}} \cdot \boldsymbol{u}^s = 0$.

Coupling at the interface Ω_{fs}

- Mass conservation (normal flux continuity): $H\boldsymbol{u} \cdot \boldsymbol{n} = H^s \boldsymbol{u}^s \cdot \boldsymbol{n}$;
- Pressure transmission (energy consistency): $\Pi = \Pi^s$, where $\Pi = \rho \mathrm{g} \zeta + \frac{1}{2}\rho|\boldsymbol{u}|^2$ and $\Pi^s = \underline{\mathrm{p}}^s - \mathrm{p}_{\mathrm{atm}} + \rho \mathrm{g} \zeta + \frac{1}{2}\rho|\boldsymbol{u}|^2$,
- Velocity compatibility (no artificial vortex): $\boldsymbol{u} \cdot \boldsymbol{n}^\perp = \boldsymbol{u}^s \cdot \boldsymbol{n}^\perp$.

A coupled "partly constrained" SW system

A first wave–structure interaction model

- Exterior region Ω_f (free surface):

$$\begin{aligned} \partial_t \zeta + \nabla_{\boldsymbol{x}} \cdot (H\boldsymbol{u}) &= 0 \\ \partial_t \boldsymbol{u} + \boldsymbol{u} \cdot \nabla_{\boldsymbol{x}} \boldsymbol{u} + \mathrm{g}\nabla_{\boldsymbol{x}} \zeta &= \boldsymbol{0} \end{aligned}$$

Nonlinear shallow-water equations

- Interior region Ω_s (under the object):

$$\begin{aligned} \nabla_{\boldsymbol{x}} \cdot \boldsymbol{u}^s &= 0 \\ \partial_t \boldsymbol{u}^s + \boldsymbol{u}^s \cdot \nabla_{\boldsymbol{x}} \boldsymbol{u}^s &= \rho^{-1} \nabla_{\boldsymbol{x}} \underline{\mathrm{p}}^s \end{aligned}$$

Incompressible Euler equations

- Interface Ω_{fs} (coupling conditions):

$$H\boldsymbol{u} \cdot \boldsymbol{n} = H^s \boldsymbol{u}^s \cdot \boldsymbol{n} \qquad \textit{Mass flux continuity}$$

$$\Pi = \Pi^s \qquad \textit{Pressure continuity}$$

$$\boldsymbol{u} \cdot \boldsymbol{n}^\perp = \boldsymbol{u}^s \cdot \boldsymbol{n}^\perp \qquad \textit{Tangential continuity}$$

Irrotational initial data: a key simplification

Propagation of irrotationality

If $\nabla_{\boldsymbol{x}}^{\perp} \cdot \boldsymbol{u}(\cdot, 0) = 0$ in Ω_f and $\nabla_{\boldsymbol{x}}^{\perp} \cdot \boldsymbol{u}^s(\cdot, 0) = 0$ in Ω_s, it stays true for all $t \geq 0$
$\hookrightarrow$ Physically the flow remains smooth, without rotation or vortex generation.

Consequence: the interior becomes elliptic

- Because the flow remains **irrotational**, the interior velocity can be written as a **gradient field** *i.e.* there exists a potential ϕ^s such that

$$\boldsymbol{u}^s = \nabla_{\boldsymbol{x}} \phi^s \quad \text{in } \Omega_s.$$

- Under the object, the free surface is fixed, hence the water depth is **constant in time**: $\partial_t H^s = \partial_t (H_0 + \zeta^{\mathrm{w}}) = 0$.
- Combining irrotationality with the incompressibility constraint $\nabla_{\boldsymbol{x}} \cdot \boldsymbol{u}^s = 0$ leads to an **elliptic problem** for the potential:

$$\nabla_{\boldsymbol{x}} \cdot \left(H^s \nabla_{\boldsymbol{x}} \phi^s \right) = 0 \quad \text{in } \Omega_s.$$

From the interior constraint to a mixed formulation

What happens under the object

- To solve $\nabla_{\boldsymbol{x}} \cdot \left(H^s \nabla_{\boldsymbol{x}} \phi^s\right) = 0$ in Ω_s, we prescribe the trace of the potential on the interface,

$$\phi^s = \psi^s \quad \text{on } \Omega_{fs}.$$

- The trace ψ^s is **not arbitrary**: it evolves in time according to an ODE obtained from the Bernoulli relation on the interface,

$$\partial_t \psi^s = -\mathrm{g}\zeta - \frac{1}{2}|\boldsymbol{u}|^2 \quad \text{on } \Omega_{fs}.$$

How the interior talks to the exterior

We define the following **Dirichlet–Neumann operator:**

$$\Lambda\psi^s := H^s \nabla_{\boldsymbol{x}} \phi^s \cdot \boldsymbol{n} \quad \text{on } \Omega_{fs},$$

maps the potential ψ^s (Dirichlet data) to the normal flux (Neumann data)
$\hookrightarrow$ Quantifies how the interior motion exchanges water with the exterior flow

A special configuration: the infinite pontoon

- The interior region is an infinite strip $\Omega_s = (-\ell, \ell) \times \mathbb{R}$, while the exterior domain consists of two half-planes $\Omega_{f\pm} = \{(x, y) \mid \pm x > \ell\}$.
- In this configuration, the **Dirichlet–Neumann operator is explicit**: no elliptic problem has to be solved inside the structure.
- This makes the infinite pontoon an **ideal benchmark**: it allows us to validate the numerical coupling independently of the interior solver.
- Moreover, for y-independent solutions, the model reduces to a known **one-dimensional wave–structure interaction system**.

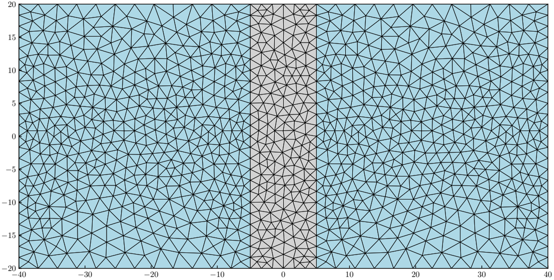

Explicit Dirichlet–Neumann operator (pontoon case)

In the infinite pontoon configuration, the interior elliptic problem can be solved **explicitly** by Fourier transform in the transverse variable y.

The generalized Dirichlet–Neumann operator can be written explicitly as:

$$\Lambda_-\boldsymbol{\psi}^s(y) = H^s\,\mathfrak{F}^{-1}\Big(\xi\coth(2\ell\xi)\,\widehat{\psi}_-(\xi)\Big)(y) - H^s\,\mathfrak{F}^{-1}\left(\frac{\xi}{\sinh(2\ell\xi)}\,\widehat{\psi}_+(\xi)\right)(y),$$

$$\Lambda_+\boldsymbol{\psi}^s(y) = -H^s\,\mathfrak{F}^{-1}\left(\frac{\xi}{\sinh(2\ell\xi)}\,\widehat{\psi}_-(\xi)\right)(y) + H^s\,\mathfrak{F}^{-1}\Big(\xi\coth(2\ell\xi)\,\widehat{\psi}_+(\xi)\Big)(y),$$

where $\boldsymbol{\psi}^s = (\psi_-, \psi_+)$ be the potentials on $x = \pm\ell$ and where $\widehat{\psi}_\pm = \mathfrak{F}(\psi_\pm)$ denotes the Fourier transform with respect to the transverse variable.

As a consequence:

- the interior elliptic problem is **fully eliminated**,
- the coupling reduces to an **explicit boundary operator** and a **boundary ODE** for $\psi_\pm$.

💡 This provides a natural benchmark for validating the numerical method!